Supplementary Information

For

Metal Organic Framework steered electrosynthesis of anisotropic gold nanorod for specific sensing of organophosphate pesticides in vegetables collected from field

Chansi[1a], Pragadeeshwara Rao R[1b], Irani Mukherjee[3], Tinku Basu*, Lalit M Bharadwaj[2]

[1a, b,*] Amity Centre for Nanomedicine, Amity University Uttar Pradesh, Noida -201303, India.

[2]Amity Institute of Nanotechnology, Amity University Uttar Pradesh, Noida -201303, India.

[3]Division of Agricultural Chemicals Indian Agricultural Research Institute New Delhi-110012, India

[*]Email ID: tbasu@amity.edu

TABLE OF CONTENTS

SI 1 Optimisation of parameters for electrochemical deposition of aAuNR morphologies

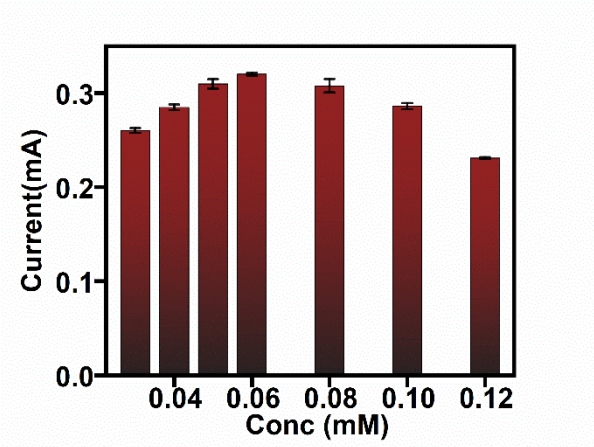

Fig. S1 Bar diagram showing anodic peak current values of CV within potential of -0.3 V to 0.8 V at a scan rate 0.1 Vs^{-1} for various electrodeposited anisotropic nano structured gold on MOF/ITO surfaces with varied concentration of $AuCl^{4-}$

Fig. S1 represents the anodic peak current response at a varied concentration of $AuCl^{4-}$ **the** salt used for the electrodeposition of gold nanostructures. At 0.06 mM concentration, the peak current response was maximum, hence used for further deposition.

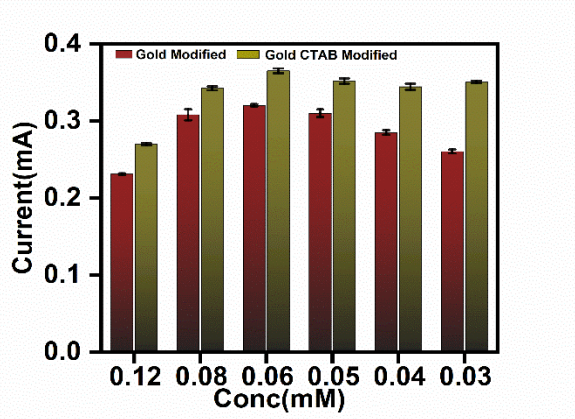

Fig. S2 Comparison of variation of anodic peak current values at different concentration of pure chloroauric acid and mixture of chloroauric acid and CTAB with1:1 ratio with AC voltage of -0.3 V to-0.8 V at a scan rate of 0.1 Vs^{-1}

Fig. S2 represents the comparison of the anodic peak current values in presence of $AuCl^{4-}$ and a similar concentration of $AuCl^{4-}$ along with CTAB at a ratio of 1:1. In presence of CTAB, the current response is higher than $AuCl^{4-}$ alone. Hence, CTAB plays a major role in the incorporation of anisotropic behavior leading to greater ion transfer.

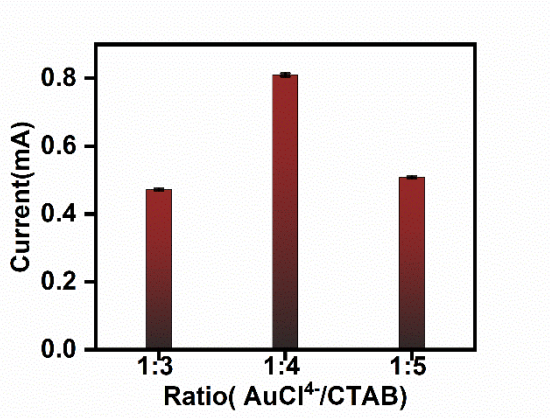

Fig. S3 Bar diagram showing the anodic peak current values response recorded at varied concentration ratio of $AuCl^{4-}$ and CTAB

Fig. S3 represents the anodic peak current response at a varied ratio of $AuCl^{4-}$ and CTAB. From the graph, it is seen that the maximum current response is recorded with a ratio of 1:4.

SI 2 Method for Detection of pesticide in spiked sample vegetable extract

Vegetables like Abelmoschus esculentus and Solanum melongena were used for the isolation of vegetable extract by the Quechers Method[1]. The bioprobe was incubated with 10 µL of spiked extract for 17 min. The spiked incubated bioprobe was tested for recovery pesticide concentration and the percentage deviation was calculated.

SI 3 Details of vegetables and pesticide for field sample study

Table S1 List of vegetables and pesticide sprayed for field sample study

Pesticide sprayed (Fortification level µg/g)	Vegetables
ethion	Momordica charantia
methyl parathion	Solanum melongena, Abelmoschus esculentus, Capsicum annuum
chlorpyrifos	Abelmoschus esculentus

SI 4 Spectroelectrochemical Studies

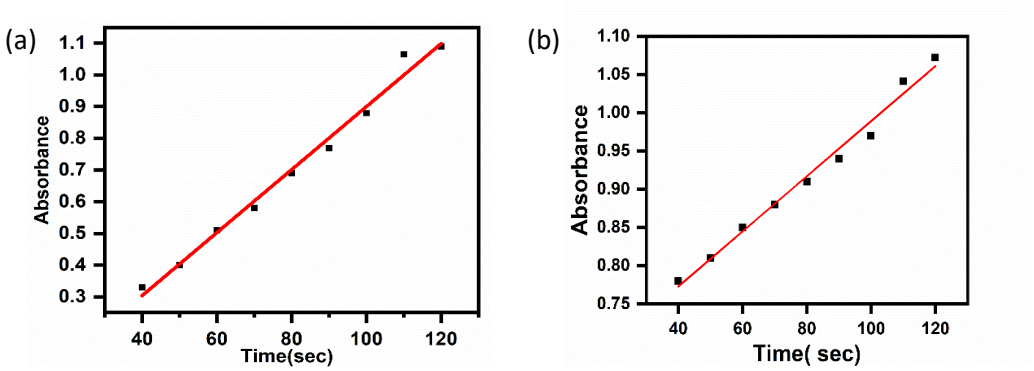

Fig. S4 Rate kinetics of growth of aAuNR nanorod growth over (a) ITO (b) MOF/ ITO studied through spectro-electrochemistry

Fig. S4 shows the rate of growth of aAuNR is recorded after 40 sec of the deposition process. It can be seen that the growth of aAuNR over the MOF/ITO surface observes high linearity (0.97) in comparison to aAuNR deposition over the ITO surface (0.96).

SI 5 Morphological Studies

SI 5.1 FESEM studies

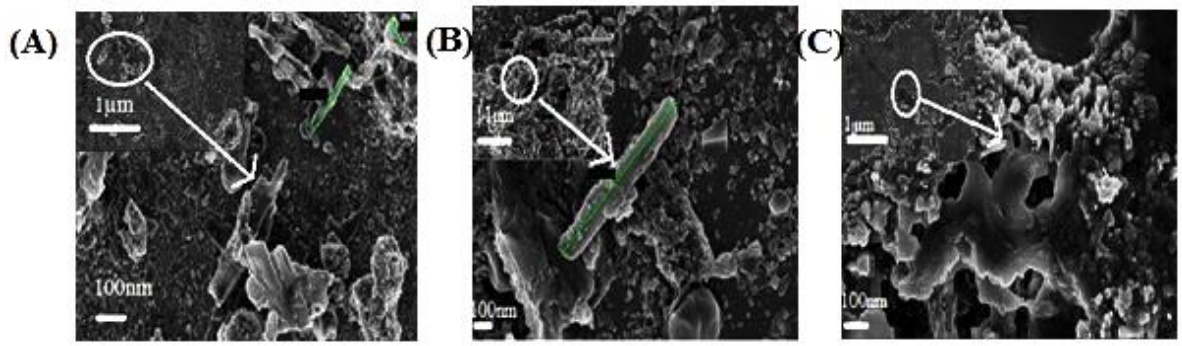

Fig. S5 FESEM micrograph of surface morphologies formed by varying aspect ratio of $AuCl^{4-}$/CTAB (A) 1:3 (B) 1:4 (C) 1:5 respectively seen at 1 µm (inset) with magnified view at 100 nm

Fig. S5 represents the surface morphology investigated by the FESEM study of aAuNR with the effect of change in the ratio of $AuCl^{4-}$ to CTAB from 1:3 to 1:5 on anisotropic morphology of gold nanostructure for the development of aAuNR/MOF/ITO surface. The surface morphology captured by the FESEM image study signifies that initiation of the formation of aAuNR on MOF/ITO surface starts at a 1:3 ratio (**Fig. S5(A)**) and finally aAuNR morphology develops at 1:4 molar ratio of $AuCl^{4-}$ and CTAB as seen in **Fig. S5(B).** With further increase in CTAB concentration, i.e., 1:5 **Fig. S5(C)** molar ratio, the deformation of anisotropy starts through agglomeration as shown in the FESEM image **Fig. S5(C**). The surface analysis reveals the optimum aspect ratio for the formation of anisotropic morphology is 1:4.

Table S2 Atomic Weight Composition of Elements in Bioprobe

Metal	Weight (%)	Atomic Weight%)
O	**21.20**	**59.03**
Zn	**17.62**	**12.00**
N	**4.93**	**15.66**
Na	**3.73**	**7.23**
C	**1.57**	**5.82**
Au	**1.12**	**0.25**

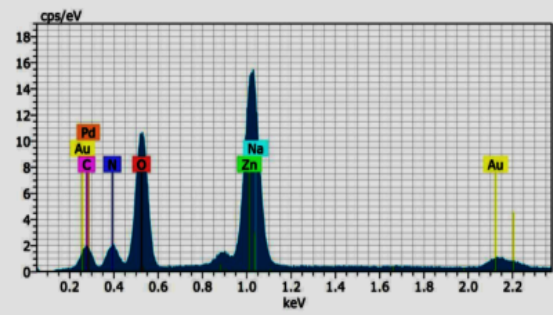

Fig. S6 EDAX analysis aAuNR/MOF/ITO surface depicting the atomic weight percentage composition of each element present on the surface

Fig. S6 represents the EDAX analysis of the as prepared aAuNR/MOF/ITO surface showing the presence of C, O, Zn, and Au analysis reveals the presence of N on the sample surface is due to the unreacted zinc nitrate and triethylamine in the MOF coating.

SI 5.2 AFM Analysis

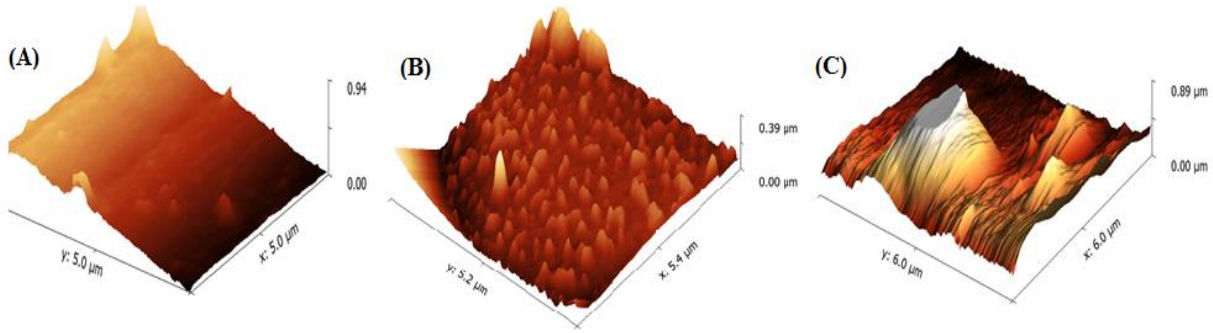

Fig. S7 AFM analysis of respective topologies of optimisation of the ratio of $AuCl^{4-}$ and CTAB for deposition of aAuNR morphologies over MOF/ITO surfaces (A) 1:3 (B) 1:4 (C) 1:5 respectively

Fig. S7 represents the AFM analysis of optimisation of the ratio of $AuCl^{4-}$ to CTAB for the formation of aAuNR nanostructures. Initiation of the formation aAuNR starts at a ratio of 1:3 (Fig. S7(A)). However, there is no clear demarcation, and the formation of nanostructures occurs. Subsequently, as the concentration of CTAB increases to a ratio of 1:4 (Fig. S7 (B)) discrete deposition of the aAuNR is visible (Fig. S7(B)). On further increase in ratio to 1:5 (Fig. S7 (C)) leads to distortion in the structure and aggregates of the salt gets deposited over the surface rather than the formation of aAuNR, Hence the optimized ratio of $AuCl^{4-}$ to CTAB is found to be 1:4 which corporates the results obtained from FESEM analysis.

SI 6 Electrochemical Characterisation of AChE/aAuNR/MOF/ITO electrode

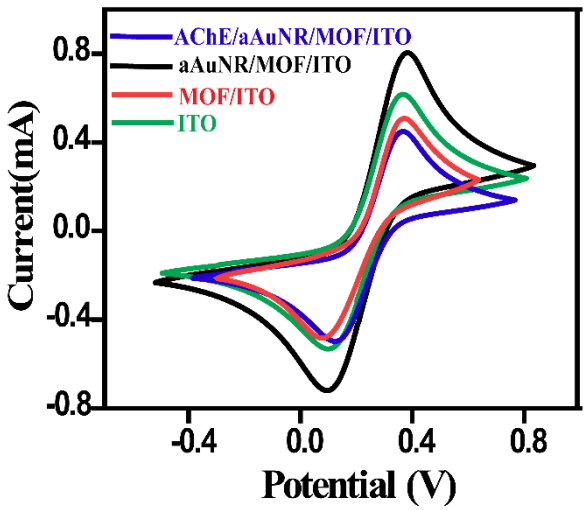

Fig.S8 CV curves of each stage of fabrication of AChE/aAuNR/MOF/ITO bioprobe (a) ITO (b) MOF/ITO (c) aAuNR/MOF/ITO (d) AChE/aAuNR/MOF/ITO

Electrochemical characterisation of AChE/aAuNR/MOF/ITO was conducted at each of fabrication. The bare electrode (ITO) being electrically conductive shows a peak current value of 0.608 mA as shown in Fig. S8. A reduction in current to a level of 0.466 mA is noticed for MOF/ITO surface due to the non-conductive nature hindering the movement of electrons over the surface of the electrode. Fig. S8, curve c represents a dramatic increase in peak current of the redox mediator to a level of 0.804 mA for electrodeposited anisotropic metal

morphologies over the previous surface signifying the significant increase in conductivity of the modified electrode offered by the deposition of conductive anisotropic nanorod morphologies (aAuNR /MOF/ITO). Immobilization of the enzyme over (aAuNR/MOF/ITO) electrode shows the decrease in the current (.404 mA) as it obstructs the flow of current.

SI 7 Response study of MOF/ITO electrode towards organophosphate pesticides

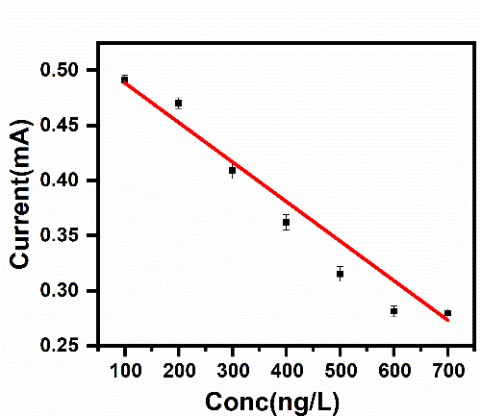

Fig. S9 Calibration curve as a plot of current versus pesticide (chlorpyrifos, malathion, methyl parathion, parathion) concentration (ng/L) for detection of OP's using MOF/ITO electrode

Fig. S9 shows the response of the MOF/ITO surface for the detection of OPs by CV. The electrodes were incubated with various concentrations of OP pesticides for 10 min for adsorption of pesticides by its porous surface. The electrodes were further washed of unbound pesticide. The anodic peak current response after washing of the pesticide was measured using CV. A linear relationship exists between anodic peak current and OP concentration within the range of 100-600 ng/L. This shows that MOF acts as a screening matrix for pesticide detection.

SI 8 Optimisation of parameters for response study

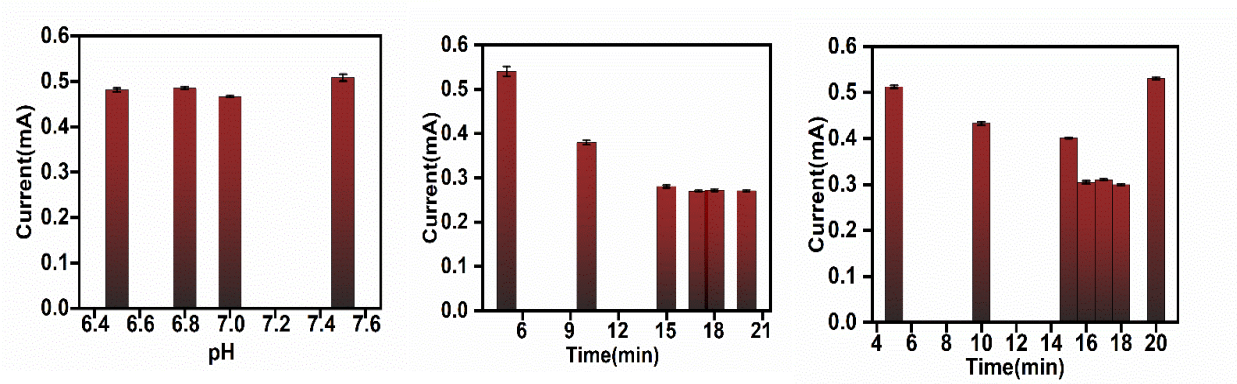

Fig.S10 Change in anodic peak current values (a) variation of pH of the solution, change in incubation time of (b) chlorpyrifos (c) malathion used for detection of pesticides

The optimum electrochemical response by the proposed bioprobe for detection of OP pesticide is obtained at pH 7.0 when the pH of the PBS used was varied from 6.5 to 7.5 recorded using three electrode cell using PBS 50 mM. Because the reduction in response current is maximum at pH 7.0 for the same concentration of OP. The optimized time required for the incubation time of various OP was deduced by varying the interaction time from 5 min to 20 min. The maximum decrease in current after the incubation of chlorpyrifos was reported for 17 min (Fig. S11(B)) and malathion was 18 min (Fig. S11(C)).

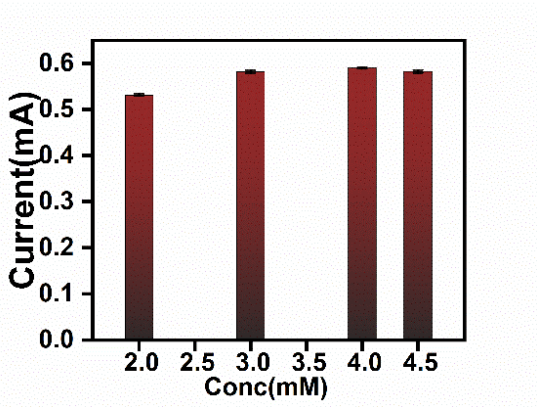

Fig. S11 shows the optimisation for the concentration of ATCl by cyclic voltammetry analysis potential of -0.3 V to 0.8 V at 0.1 Vs^{-1} by varying the concentration at fixed enzyme concentration (1 $mgmL^{-1}$)

The response of the electrode depends on the inhibition of the enzyme AChE activity towards the substrate ATCl, so its concentration is to be optimized to study the response of the sensor effectively. The concentration was varied from 2 mM to 4 mM and the cyclic voltammetric response at fixed enzyme concentration 1 $mgml^{-1}$ was recorded. The current sensitivity was maximum for 4 mM ATCl further increase in concentration causes saturation, no increase in current further. Hence, this concentration of ATCl was used for the entire study.

SI 9 Inhibition Rate Kinetic Study

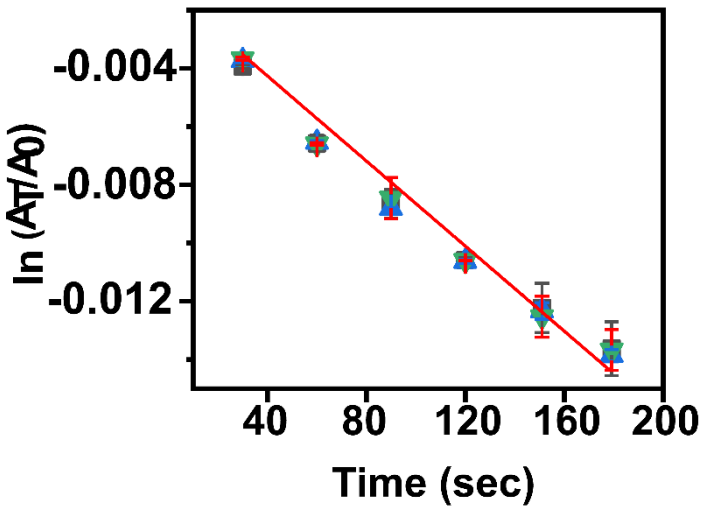

Fig.S12 Kinetic study to measure the inhibition of acetylcholinestrase by various OP's (graph between ln (A_T/A_0 vs Time (t in sec)

As the rate constant of inhibition reaction is determined by the addition of the substrate. The rate of inhibition of AChE follows pseudo-first-order rate kinetics and the rate of reaction is determined by:

$$\text{Ln } (A_T/A_o)=-kt$$

A_T = Absorbance of the different time interval

A_o= Absorbance at 0 min

The graph plotted between $l_n [A_T/A_O]$ with the function of time for chlorpyrifos, methyl parathion, and malathion and slope of the graph describe the rate constant k (-ve sign in value of k is due to inhibition reaction)The rate constant of each reaction is summarised in the table below.

Table S3 Inhibition rate constant for different OP's

Pesticide	**K (sec^{-1})**
chlorpyrifos	-4.8×10^{-5}
malathion	-4.798×10^{-5}
methyl parathion	-4.796×10^{-5}

Since the value of the rate constant nearly the same $=-4.8 \times 10^{-5}$, hence the inhibition reaction proceeds at the same rate for all OP s irrespective of their structures

SI 10 Interference Studies

Apart from heavy metals (Pb^{2+}, Cu^{2+}, Zn^{2+}), inorganic phosphate (an active component of fertilizers), aflatoxinB1 a major mycotoxin[2], diisopropylfluoro phosphate (a component of nerve agent and drugs)[3] inhibit AChE activity, so they were tested as interferents. Equal concentration of OP along with these interferents was tested and the result is reported in Fig. S14. The percentage interference was calculated and the maximum interference % was reported as 4.3% for inorganic phosphate, 4.8% aflatoxin B1, 5.5% for diisopropyl phosphate respectively.

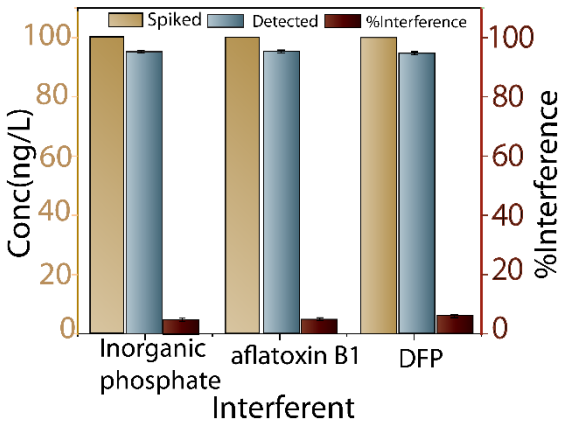

Fig. S13 Bar diagram showing the interference of heavy metals along with pesticide on detection of pesticide by AChE/Cys/aAuNR/MOF/ITO

SI 11 Aqueous Stability study of MOF-5/ITO electrode

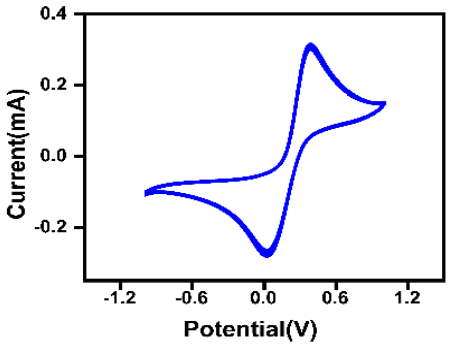

Fig. S14 Repeated CV response of MOF/ITO electrode for 2 min within potential (-1 V to 1 V) at 0.1V/s scan rate

Fig. S14 represents CV response of MOF/ITO electrode for 25 cycles (120 sec) within potential (-1 V to 1 V) at 0.1V/s scan rate using PBS(pH=7), 50 mM, 0.9% (w/v) NaCl containing 5 mM $[Fe(CN)_6]^{3-/4-}$ as a redox species. The voltagramms as obtained were plotted and a negligible variation in the anodic peak current was noticed confirming that during the synthesis of anisotropic gold nanostructure and electrochemical sensing of OP, stability, and integrity of MOF structure is maintained.

SI 12 Detection of pesticide in spiked samples

Table S4 Represent the response study of the developed bioprobe towards detection of spiked pesticide (chlorpyrifos) in vegetable (Abelmoschus esculentus) extract

Sample Spiked (ngL^{-1})	Sample detected by LCMS/MS (ngL^{-1})	Sample detected by developed Sensor Electrode (ngL^{-1})
500	420	400
100	80	70

SI 13 Detection of Pesticide in field sample vegetable Extract

Table S5 Detection of Pesticide (chlorpyrifos, methyl parathion, ethion) in Vegetable extract (Abelmoschus esculentus, Capsicum annuum, Momordica charantia) taken at regular Interval

Pesticide	Vegetable	Day	Sample Detected by Sensor Electrode(ngL^{-1})	Sample detected by GC/ECD (ngL^{-1})	Error
chlorpyrifos	Abelmoschus esculentus	3rd	100	95.80	+4.1%
		5th	80	78	+2.56%
		7th	50	45.20	+9.75%
		15th	30	24.84	+17.2%
methyl parathion	Solanum melongena	3rd	380	362	+5%
		5th	255	246	+4%
		7th	138	128	+8%
		15th	92	80	+16%
	Capsicum annuum	3rd	340	322	+6.2%
		5th	228	209	+9.1%
		10th	122	111	+10.1
		15th	72	62	+16.1%
ethion	Momordica charantia	3rd	392	369.3	+6%
		5th	284	261.3	+9%
		10th	190	169.3	12%
		15th	92	80	+16%

SI 14 In silico studies

We have performed in silico blind docking study to understand the molecular mechanism underlying the interaction of various OP's (having different functional groups) towards AChE. Six different OP's chlorpyrifos, malathion, methyl parathion, parathion, ethion, profenofos) were subjected to the docking analysis against the AChE receptor proteins from electrophorus electricus with PDB ID: 1C2O. Using a rigid receptor and flexible ligand model, docking results were obtained from Autodock Vina

The ligands were ranked according to the average binding energy obtained from different poses of each ligand. The average rankings are -5.9 kcal/mol for chlorpyrifos, -5.8 kcal/mol for profenofos -5.7 kcal/mol for methyl-parathion, -5.6 kcal/mol for parathion, -5.3 kcal/mol for malathion, and -4.02 kcal/mol for ethion.

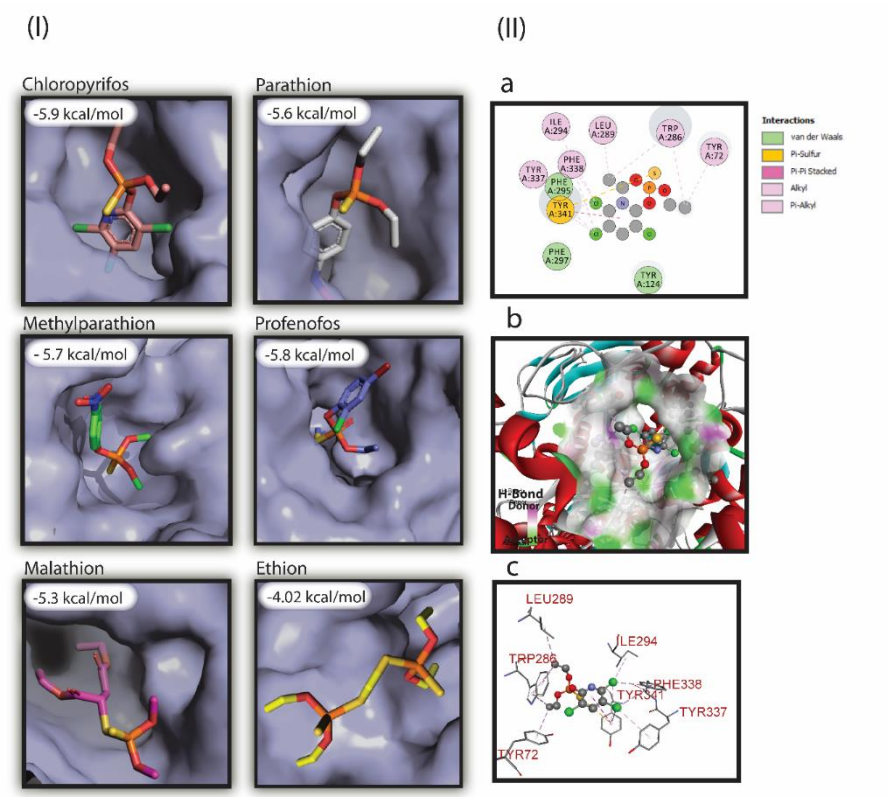

Fig.S15 (I) Docking poses of all the six OPs tested (II)(a-c), shows the 2D, H-bond donor acceptor interaction maps and 3D interaction of cpf with AChE receptor

Fig. S15(I), shows the docking poses of all the six OPs tested and Fig. 5II(a-c), shows the 2D, H-bond donor acceptor interaction maps and 3D interaction of chlorpyrifos with AChE receptor, respectively. It is envisaged that amongst the six OPs tested, chlorpyrifos and profenofos exhibit the highest binding energy (-5.9 kcal/mol) whereas ethion (-4.1kcal/mol) has the lowest AChE activity. chlorpyrifos demonstrates π-S bonding with TYR341 (5.32 Å), π-π stacking with TYR341(4.86 Å), π-cation with trp228 (4.7 Å), π-alkyl interaction with tyr124 (4.38 Å), tyr72 (4.65 Å), and alkyl bond linking ile294 (4.39 Å), phe338 (4.94 Å), phe338 (4.52 Å), tyr337(4.71 Å) respectively (Fig. S15). profenofos supports π-S bonding with TYR341(5.41 Å), π-π stacking with TYR341 (4.90 Å), π-alkyl interaction with tyr337 (4.48 Å), PHE338 (4.68 Å), and alkyl bond linking LEU76 (3.66 Å), TYR341 (4.65 Å). On comparing chlorpyrifos with profenofos, chlorpyrifos has a shorter bond length whereas profenofos has a longer bond length with more hydrophobic interactions with the docked receptor, conforming its strongest interaction of chlorpyrifos among six OPs tested. H-bond donor-acceptor interaction, 2D maps, and 3D visualization of each OP scored are presented in Fig. S16(a-f). The theoretically calculated inhibition constant(K) of chlorpyrifos is found to be the highest as 5.38×10^{-5} M also substantiates strong affinity towards AChE (Details of inhibition constant of various OP are provided in Table S4). Table S6 and S7 present the binding affinity and RMSD values respectively for each OP molecule obtained from Autodock vina output. Physiochemical properties of all OP as calculated in reported in Table S8.

Further site-specific docking studies were performed and detailed results for the same is shown in Fig. S1, Table S9-10

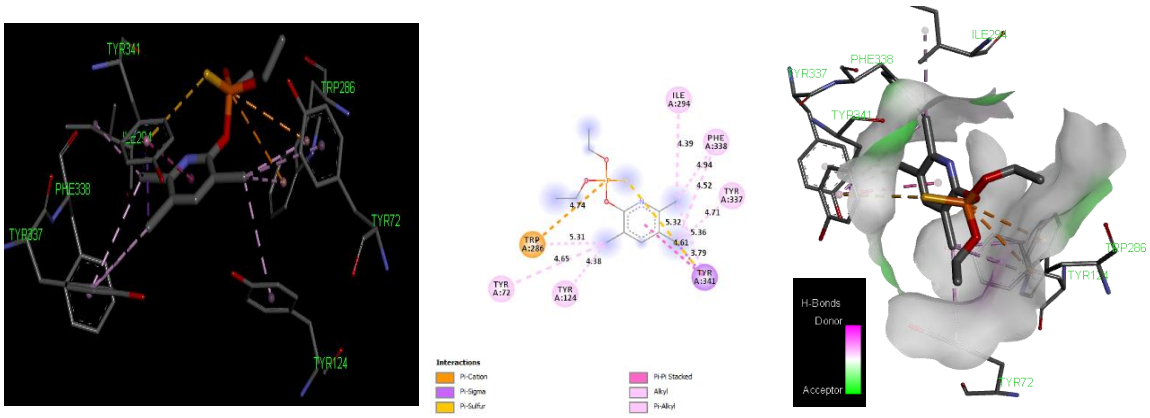

Fig.S16 (a) Molecular docking graphics of chlorpyrifos showing docking site pose, 2D hydrogen bonds

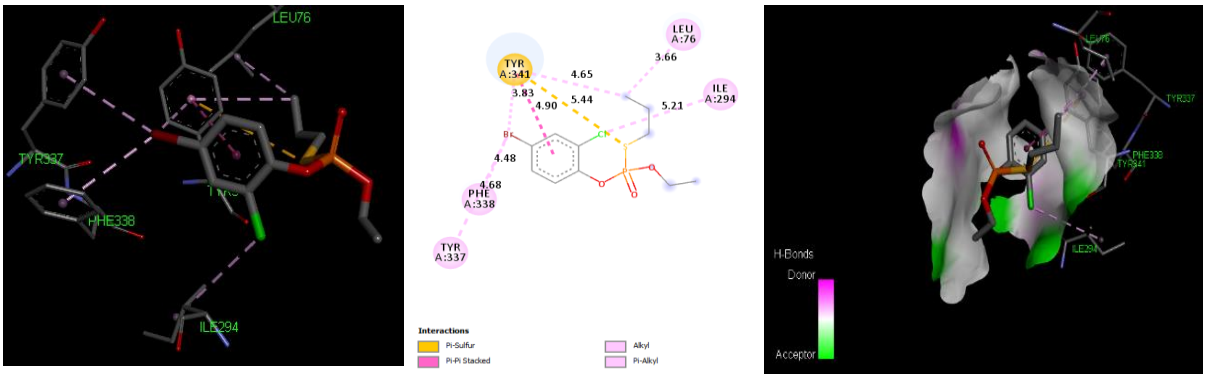

Fig.S16 (b) Molecular docking graphics of profenofos showing docking site pose, 2D hydrogen bonds

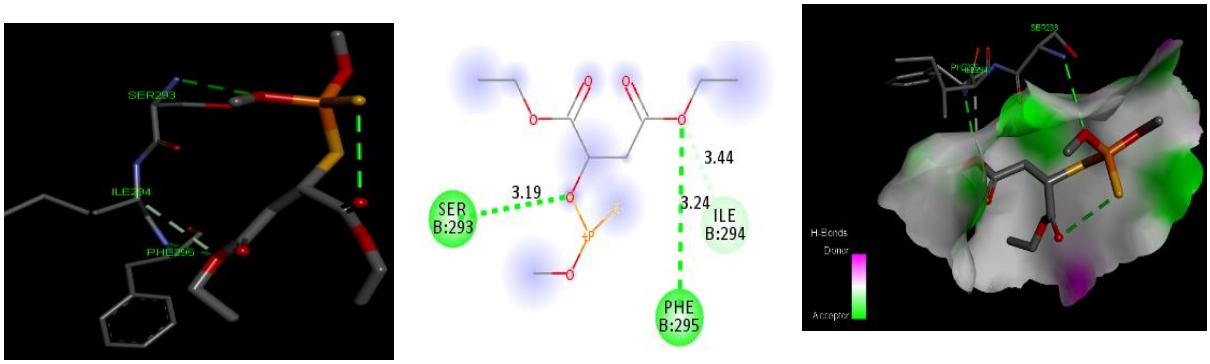

Fig.S16 (c) Molecular docking graphics of malathion showing docking site pose, 2D hydrogen bonds

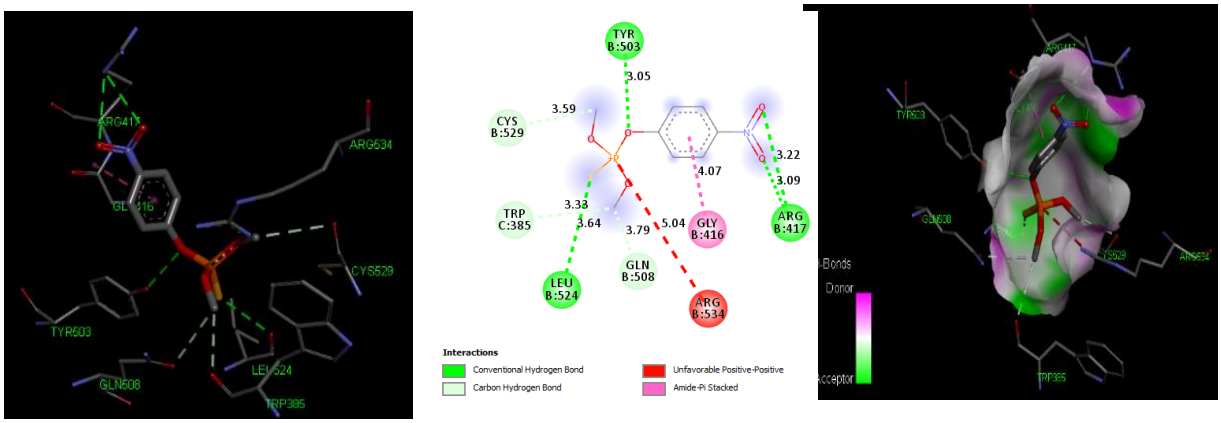

Fig.S17 (d) Molecular docking graphics of parathion showing docking site pose, 2D hydrogen bonds

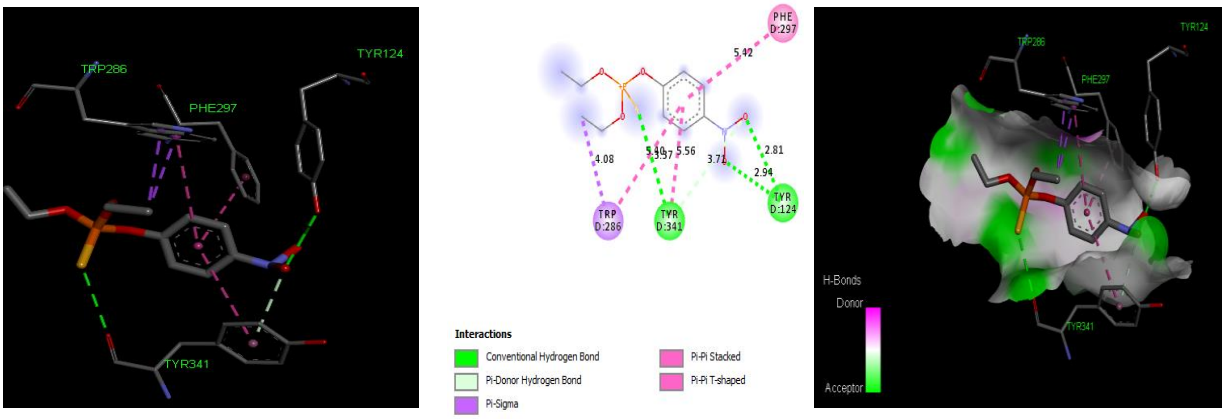

Fig.S16 (e) Molecular docking graphics of methyl parathion showing docking site pose, 2D hydrogen bonds

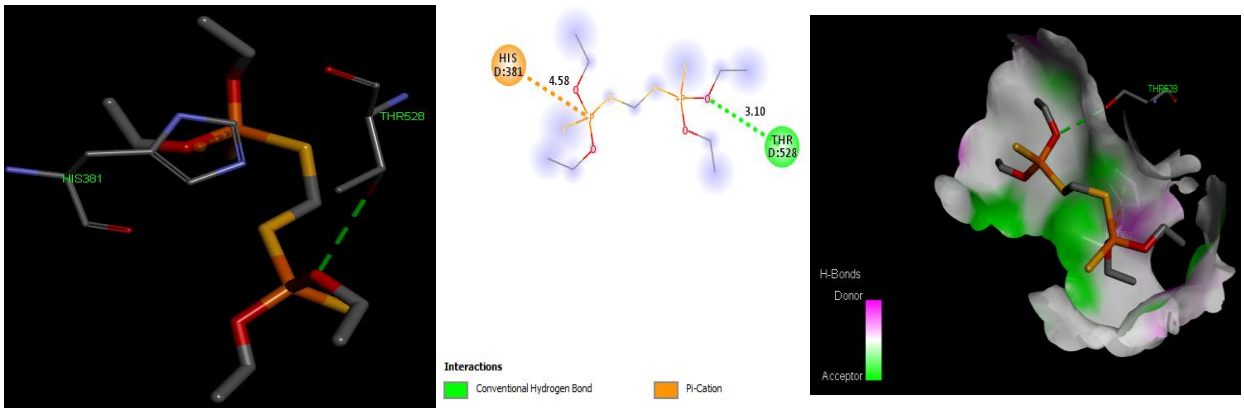

Fig. S16 (f) Molecular docking graph showing ethion docking site pose, 2D hydrogen bonds

Table S6 Molecular docking results with effective Vanderwal interactions

Pesticide	DELTA G	H BOND	PI-SULFUR	PI-PI STACK	PI-CATION	PI-ALKYL	ALKYL	AMIDE pi-stack
Chlorpyrifos	-5.9	-	5.32(TYR 341)	4.61(TYR 341)	4.74(TRP 286)	4.38(TYR124) 4.65 (TYR A:72)	4.39(ILE294) 4.94(PHE338) 4.52(PHE338) 4.71(TYR 337)	
profenofos	-5.8	-	5.44(TYR 341)	4.90 (TYR 341)		4.68 (PHE338) 4.48(TYR 337)	3.66(LEU 76) 4.65(TYR 341)	
malathion	-5.5	3.24 (PHE 295) 3.19(SER 293)	-	-				
parathion	-5.8	5.40(TYR 341) 2.94(TYR 124) 2.81 (TYR 124)	-	5.40(TRP 286) 5.56 (TYR 341) 5.42 (PHE 297)	-	-		
methyl parathion	-5.8	3.05(TYR 503) 3.64 (LEU 524) 3.22(ARG 417)	-	-				4.07(GLY 416)
Ethion	-4.1	3.10(THR 528)	-	-	4.58(HIS 381)			

Table S7 Representation of auto-dock vina results showing rmsd and inhibition constant values

Pubchem Id	LIGAND	Auto-dock Vina Results
PDB ID: IC2O	Chlorpyrifos	mode | affinity | dist from best mode | (kcal/mol) | rmsd l.b.| rmsd u.b. -----+------------+----------+---------- 1 -6.3 0.000 0.000 2 -6.1 1.542 3.169 3 -6.1 58.701 59.853 4 -6.1 47.237 48.322 5 -5.9 47.262 48.398 6 -5.8 19.417 20.329 7 -5.8 59.106 60.253 8 -5.8 40.776 41.988 K=2.38 X 10^{-5} M
	profenofos	mode | affinity | dist from best mode | (kcal/mol) | rmsd l.b.| rmsd u.b. -----+------------+----------+---------- 1 -6.3 0.000 0.000

		2 -6.0 4.015 6.153 3 -6.0 45.066 47.453 4 -5.9 3.913 6.060 5 -5.8 4.183 6.457 6 -5.8 45.006 47.518 7 -5.7 58.980 60.338 8 -5.6 44.456 46.954 9 -5.5 57.379 58.472 K=2.38 X 10^{-5} M
	methyl parathion	mode | affinity | dist from best mode | (kcal/mol) | rmsd l.b.| rmsd u.b. -----+------------+----------+---------- 1 -6.0 0.000 0.000 2 -5.9 37.196 38.403 3 -5.8 70.953 71.832 4 -5.8 28.068 29.178 5 -5.7 53.184 56.060 6 -5.6 29.173 30.376 7 -5.6 51.589 54.442 8 -5.6 36.197 37.709 9 -5.5 71.257 72.477 K=3.95X 10^{-5} M
	parathion	mode | affinity | dist from best mode | (kcal/mol) | rmsd l.b.| rmsd u.b. -----+------------+----------+---------- 1 -6.2 0.000 0.000 2 -5.9 45.921 48.496 3 -5.9 46.103 48.234 4 -5.8 44.616 47.248 5 -5.5 46.793 48.036 6 -5.4 46.162 48.454 7 -5.4 46.207 48.694 8 -5.3 45.918 47.406 9 -5.3 39.993 40.773 K=2.82 X 10^{-5} M
	malathion	mode | affinity | dist from best mode | (kcal/mol) | rmsd l.b.| rmsd u.b. -----+------------+----------+---------- 1 -5.6 0.000 0.000 2 -5.6 54.677 56.165 3 -5.5 45.448 47.950 4 -5.4 51.866 54.114 5 -5.4 45.004 46.733 6 -5.2 42.077 45.270 7 -5.2 57.157 58.796 8 -5.2 51.647 53.726 9 -5.1 31.685 34.042 K=7.77 X 10^{-5} M
	Ethion	mode | affinity | dist from best mode | (kcal/mol) | rmsd l.b.| rmsd u.b. -----+------------+----------+----------

		1 -4.3 0.000 0.000 2 -4.2 26.637 29.307 3 -4.1 67.434 69.104 4 -4.0 26.291 28.049 5 -4.0 68.469 70.239 6 -3.9 36.502 38.340 7 -3.9 69.200 70.895 8 -3.9 26.924 29.208 9 -3.9 67.988 69.324 K=6.997.77 X 10^{-4} M

Table S8 Calculated physicochemical properties of the pesticides

Pesticide	Polar surface area(2D)	Partition (log P)	H-bond Acceptor count	H-bond Donor count
chlorpyrifos	82.48	4.78	5	0
profenofos	70.64	4.88	3	0
malathion	138.26	1.86	3	0
parathion	112.73	3.32	3	0
methyl parathion	112.73	2.60	3	0
Ethion	171.32	3.93	2	0

Table S9 Molecular docking results of Site-specific docking from autodock vina with effective Vanderwal interactions

Pesticide	Delta G binding energy	H-Bond	Pi-Sulfur	Pi-Pi stack	alkyl	Pi-Alkyl
chlorpyrifos	-6.4	3.244698(PHE295) 3.588127(TYR341)		5.901877(TRP286) 4.887293(TRP286) 5.196028(TYR341)	4.383899(LEU289)	3.742414(TRP286) 5.388162(TYR337) 3.623317(TYR341)
profenofos	-6.0	3.565751(HIS447) 3.475805(SER125)		4.963931(TRP86) 5.864198(TRP86) 5.905145(TYR124)		3.769906(TRP86) 5.307700(TRP86) 5.124332(TYR337) 4.680093(PHE338)
malathion	-5.2	3.553902(GLN291) 3.598611(SER293)				5.457270(TYR124) 5.132200(PHE297) 5.178987(PHE338)
parathion	-6.3	3.680975(SER293) 3.784512(TYR341)		5.410546(TYR341) 5.130543(TRP286) 5.860532(PHE297)		
methyl parathion	-5.9	3.042336(TYR124) 3.616874(TRP286) 4.038106(TRP286) 4.033714(TRP286)		5.434852(TYR341) 5.502432(TRP286) 5.422266(PHE297)		
Ethion	-4.8	2.750655(TYR72) 3.63760(SER293) 3.521865(ARG296)	5.476318(TYR341)		4.819349(LEU289) 4.284038(LEU76) 5.067140(TRP286) 4.905706(TRP286)	3.926253(TYR72)

Table S10 Representation of site-specific auto-dock vina results showing rmsd and binding affinity values

Pubchem Id PDB ID: IC2O **(Chain C)**	**Ligand**	**Site-specific autodock vina results**
	chlorpyrifos	mode | affinity | dist from best mode | (kcal/mol) | rmsd l.b.| rmsd u.b. -----+------------+----------+---------- 1 -6.9 0.000 0.000 2 -6.5 5.314 6.982 3 -6.5 7.836 9.495 4 -6.4 7.677 9.410 5 -6.4 1.932 3.349 6 -6.2 19.897 20.805 7 -6.2 8.153 10.220 8 -6.1 8.186 9.884 9 -6.1 7.771 9.455 K= 2.012 e^{-5} M
	profenofos	mode | affinity | dist from best mode | (kcal/mol) | rmsd l.b.| rmsd u.b. -----+------------+----------+---------- 1 -6.5 0.000 0.000 2 -6.4 2.184 3.461 3 -6.3 2.950 3.755 4 -6.1 4.245 6.585 5 -6.0 4.449 6.967 6 -5.9 4.401 6.728 7 -5.8 3.568 5.578 8 -5.8 2.906 3.918 9 -5.7 6.218 8.191 K= 3.95446e^{-5} M
	malathion	mode | affinity | dist from best mode | (kcal/mol) | rmsd l.b.| rmsd u.b. -----+------------+----------+---------- 1 -5.6 0.000 0.000 2 -5.5 1.181 1.306 3 -5.4 3.202 5.555 4 -5.3 17.109 18.650 5 -5.2 3.653 5.559 6 -5.1 10.205 11.881 7 -5.1 17.895 19.482 8 -5.1 17.763 19.693 9 -5.1 1.927 2.135 K= 1.52807e^{-4}M
	parathion	mode | affinity | dist from best mode | (kcal/mol) | rmsd l.b.| rmsd u.b. -----+------------+----------+---------- 1 -6.8 0.000 0.000 2 -6.5 4.756 6.582 3 -6.4 4.965 8.396 4 -6.4 5.048 8.363 5 -6.2 3.452 6.827 6 -6.1 5.185 8.675 7 -6.1 4.824 7.476 8 -6.1 4.980 8.769 9 -6.1 5.526 8.604

		K=2.382e^{-5}M
	methyl parathion	mode | affinity | dist from best mode | (kcal/mol) | rmsd l.b.| rmsd u.b. -----+------------+----------+---------- 1 -6.7 0.000 0.000 2 -6.1 5.029 6.767 3 -6.0 4.236 5.868 4 -5.9 3.587 6.038 5 -5.9 1.264 2.203 6 -5.8 8.860 10.067 7 -5.8 6.074 6.891 8 -5.8 8.867 9.985 9 -5.8 8.863 9.860 K=4.682e^{-5}M
	ethion	mode | affinity | dist from best mode | (kcal/mol) | rmsd l.b.| rmsd u.b. -----+------------+----------+---------- 1 -5.3 0.000 0.000 2 -5.2 2.271 2.728 3 -5.0 2.609 3.541 4 -4.9 2.618 3.639 5 -4.7 2.205 3.523 6 -4.7 5.844 8.485 7 -4.7 18.644 20.191 8 -4.6 5.570 8.112 9 -4.5 6.786 8.792 K=3.00379e^{-4}M

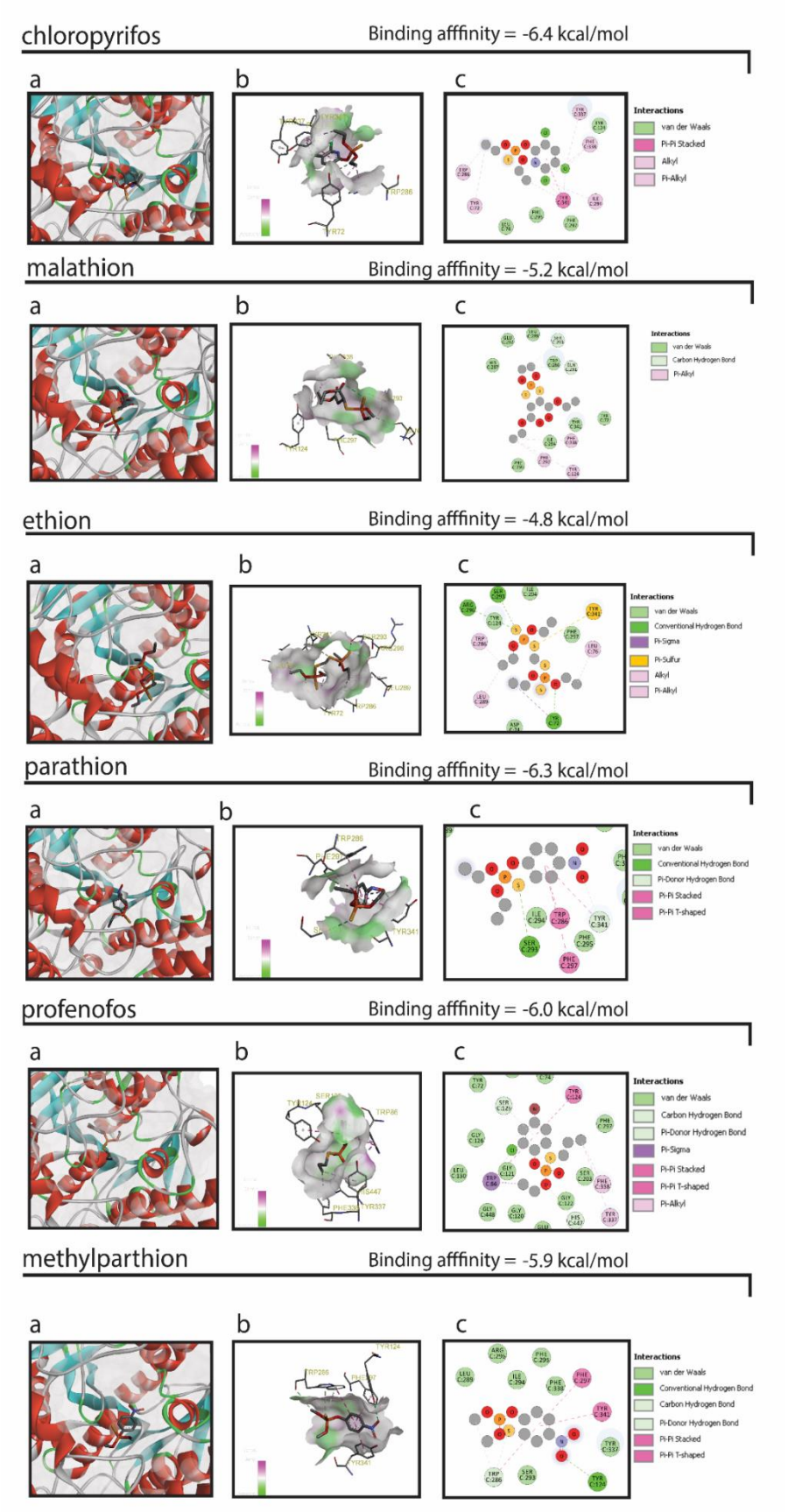

Fig. S17 Molecular docking graphics of pesticides for site-specific docking showing docking site pose, 2D hydrogen bonds

Bibliography

1 E. Boes, R. T. Rosmalina, Y. S. Ridwan, W. C. Nugraha and R. Yusiasih, *Procedia Chem.*, 2015, **16**, 229–236.

2 A. Chrouda, K. Zinoubi, R. Soltane, N. Alzahrani, G. Osman, Y. O. Al-Ghamdi, S. Qari, A. Al mahri, F. K. Algethami, H. Majdoub and N. J. Renault, *Toxins (Basel).*, 2020, **12**, 1–13.

3 E. H. Hanneman, *J. Exp. Zool.*, 1992, **263**, 41–53.